Cross second virial coefficient and dilute gas transport properties of the (H_2O + CO_2) system from first-principles calculations

Robert Hellmann*

Institut für Chemie, Universität Rostock, 18059 Rostock, Germany

Abstract

The cross second virial coefficient and three dilute gas transport properties (shear viscosity, thermal conductivity, and binary diffusion coefficient) of mixtures of water (H_2O) and carbon dioxide (CO_2) were calculated with high accuracy for temperatures up to 2000 K using statistical thermodynamics and the kinetic theory of molecular gases, respectively. The required intermolecular potential energy surface (PES) for the H_2O–CO_2 interaction is presented in this work, while the like-species interactions were modeled using PESs from the literature. All three PESs are based on high-level quantum-chemical *ab initio* computations. The predicted values for the cross second virial coefficient are in satisfying agreement with the best experimental data. In the case of the transport properties, the calculated values should be more accurate than the few available data sets.

Keywords: water, carbon dioxide, potential energy surface, second virial coefficient, transport property

The published article is available at https://doi.org/10.1016/j.fluid.2018.11.033.

1. Introduction

The calculation of the thermophysical properties of a fluid requires knowledge of the potential energy surface (PES) describing the interactions between the molecules. In the dilute gas limit, the thermophysical properties are determined only by binary interactions and thus by the pair PESs. Today, accurate pair potentials can be constructed for interactions between simple molecules such as hydrogen (H_2) [1], nitrogen (N_2) [2], carbon dioxide (CO_2) [3], water (H_2O) [4, 5], and hydrogen sulfide (H_2S) [6] by fitting suitable analytical functions to interaction energies obtained from high-level quantum-chemical *ab initio* (i.e., first-principles) calculations. If the pair potential functions are available, it is usually straightforward to evaluate second virial and cross second virial coefficients employing standard expressions from statistical thermodynamics, while the dilute gas transport properties are accessible through the kinetic theory of molecular gases [7–13].

The thermophysical properties of gaseous mixtures of H_2O and CO_2 are of importance in a number of areas, such as industrial processes related to flue gas (particularly carbon capture and storage), geothermal steam, and natural gas as well as combustion and atmospheric modeling. However, despite their practical relevance, thermophysical property data for this mixture in the gas phase are scarce, especially in the case of the transport properties. For example, there are virtually no experimental data for the shear viscosity.

In the present study, we determined reliable values for the cross second virial coefficient and the dilute gas shear viscosity, thermal conductivity, and binary diffusion coefficient of the (H_2O + CO_2) system at temperatures up to 2000 K using the same methodology as in our work on the mixtures (CH_4 + N_2) [10, 12], (CH_4 + CO_2) [13], (CH_4 + H_2S) [13], (H_2S + CO_2) [13], (CH_4 + C_3H_8) [14], (CO_2 + C_3H_8) [14], (CO_2 + N_2) [15], and (H_2S + N_2) [16]. The required PES for the H_2O–CO_2 interaction was developed as part of this study utilizing state-of-the-art quantum-chemical *ab initio* approaches. It extends much further into the highly repulsive region at small intermolecular separations than previous H_2O–CO_2 *ab initio* PESs [17–19], which is crucial for the transport property calculations. The transport properties depend also on the like-species interactions; the relevant quantities, so-called generalized cross sections (see Section 3.2), were obtained in our studies on pure H_2O [11, 20] and pure CO_2 [3] also from high-quality *ab initio* potentials [3–5].

This paper is organized as follows: The new H_2O–CO_2 PES is presented in Section 2. The computational methodologies applied to determine the thermophysical properties are summarized in Section 3. The results are presented and discussed in Section 4, and practical correlations for the cross second virial coefficient and the binary diffusion coefficient are provided in Section 5. Finally, conclusions are given in Section 6.

*Corresponding author
Email address: robert.hellmann@uni-rostock.de (Robert Hellmann)

2. H_2O–CO_2 intermolecular potential energy surface

2.1. Calculation of interaction energies

The H_2O and CO_2 molecules were treated as rigid rotors in all quantum-chemical *ab initio* calculations of H_2O–CO_2 interaction energies. The H_2O geometry is characterized by a bond length of 0.9716257 Å and a bond angle of 104.69° [21]. These values pertain to the zero-point vibrationally averaged structure and were also used by Bukowski et al. [4, 5] for their H_2O–H_2O potential. For CO_2, we used the zero-point vibrationally averaged geometry determined in our work on the CO_2–CO_2 potential [3]. It is characterized by a bond length of 1.1625 Å and a bond angle of 180°. Each H_2O–CO_2 configuration can be expressed in terms of internal coordinates by the separation between the centers of mass of the molecules, R, and four Euler angles, whose precise definition is provided in the Supporting Information.

A total of 1000 distinct angular orientations resulting from a regular grid in the four Euler angles was investigated. The region close to the only minimum of the PES (whose angular orientation is part of the regular grid) was sampled more densely by adding 12 further angular orientations. For each orientation, 24 center-of-mass separations R in the range from (1.5 to 15.0) Å were considered, resulting in 24,288 (1012×24) H_2O–CO_2 configurations. However, 1707 configurations with small R values were discarded because of excessive overlap of the two molecules or because of problems in the quantum-chemical *ab initio* calculations related to near-linear dependencies in the basis sets, leaving 22,581 configurations.

Interaction energies V for all configurations were obtained from counterpoise-corrected [22] supermolecular calculations. First, such calculations were performed at the frozen-core resolution of identity second-order Møller–Plesset perturbation theory (RI-MP2) [23, 24] level with the RI-JK approximation [25, 26] for the Hartree–Fock (HF) step. In these calculations, the aug-cc-pVXZ [27, 28] basis sets with $X = 4$ (Q) and $X = 5$ were used in conjunction with the auxiliary basis sets aug-cc-pV5Z-JKFIT [29] and aug-cc-pV5Z-MP2FIT [30] for both basis set levels. In addition, bond functions were placed midway along the R axis of each configuration, which, following Patkowski [31], were chosen to be the hydrogenic functions of the respective basis set and auxiliary basis set levels as for the other atoms. Differences between interaction energies obtained with the RI-MP2 method and the standard MP2 approach are negligibly small, but the RI-MP2 method is significantly faster. The correlation parts of the computed interaction energies, $V_{\text{RI-MP2 corr}}$, were extrapolated to the complete basis set (CBS) limit using the two-point scheme recommended by Halkier et al. [32],

$$V_{\text{RI-MP2 corr}}(X) = V^{\text{CBS}}_{\text{RI-MP2 corr}} + \alpha X^{-3}. \tag{1}$$

The HF contributions were taken from the RI-MP2 calculations at the $X = 5$ basis set level, for which they are effectively converged. In the next step, counterpoise-corrected supermolecular calculations were performed also at the frozen-core coupled-cluster level with single, double, and perturbative triple excitations [CCSD(T)] [33] employing the aug-cc-pVTZ and aug-cc-pVQZ basis sets (in both cases without the above-mentioned bond functions) for all configurations. The differences between the CCSD(T) and MP2 interaction energies [the latter obtained as a byproduct of the CCSD(T) computations] were extrapolated to the CBS limit in the same way as $V_{\text{RI-MP2 corr}}$ and then added to $V^{\text{CBS}}_{\text{RI-MP2}}$. In the well region of the PES, the interaction energies V thus obtained should correspond very closely to the frozen-core CCSD(T)/CBS level, probably to within about ±1%.

The detailed results of the *ab initio* calculations for all 22,581 investigated configurations are listed in the Supporting Information. The RI-MP2 and CCSD(T) calculations were performed using ORCA 3.0.3 [34] and CFOUR [35], respectively.

2.2. Analytical potential function

A site–site potential function with isotropic site–site interactions was fitted to the computed interaction energies. The number of sites was chosen to be nine for H_2O and seven for CO_2. Due to symmetry, there are four types of sites in CO_2. In the H_2O molecule, all sites were placed in the molecular plane, with three of them being on the symmetry axis. This arrangement, which was found to yield the best fit quality, results in six types of sites for H_2O. Thus, we have 24 distinct site–site combinations and 63 site–site interactions in total. Each of these is represented by

$$V_{ij}(R_{ij}) = A_{ij}\exp(-\alpha_{ij}R_{ij}) - f_6(b_{ij}, R_{ij})\frac{C_{6\,ij}}{R_{ij}^6} + \frac{q_i q_j}{R_{ij}}, \tag{2}$$

where R_{ij} is the separation between site i in H_2O and site j in CO_2, and f_6 is a damping function [36],

$$f_6(b_{ij}, R_{ij}) = 1 - \exp(-b_{ij}R_{ij})\sum_{k=0}^{6}\frac{(b_{ij}R_{ij})^k}{k!}. \tag{3}$$

The total interaction potential is then obtained as

$$V = \sum_{i=1}^{9}\sum_{j=1}^{7} V_{ij}(R_{ij}). \tag{4}$$

The parameters A, α, b, and C_6 for the 24 distinct site–site combinations, the positions of the sites within the molecules, and the site charges q (fixed at zero for one of the H_2O sites and two of the CO_2 sites) were optimized in a non-linear least-squares fit to the *ab initio* calculated interaction energies using a weighting function w given by

$$w = \frac{\exp\left[0.002\left(R/\text{Å}\right)^3\right]}{\left[1 + 5\times10^{-7}\left(V/\text{K} + 1500\right)^2\right]^2}. \tag{5}$$

The denominator of this function causes the weight of configurations to increase as the interaction energy decreases toward its most negative values ($V > -1500$ K for all investigated configurations), while the numerator ensures a high fit quality at large

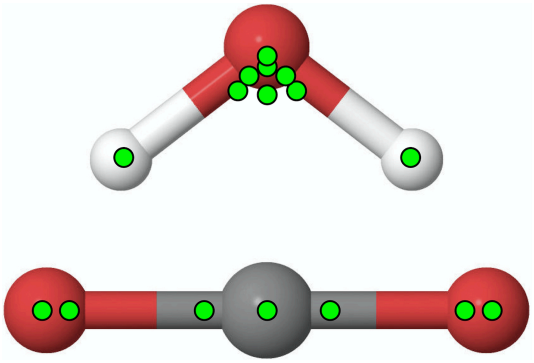

Figure 1: Visualization of the optimized positions of the nine interaction sites for H_2O and the seven interaction sites for CO_2. All H_2O sites are in the molecular plane.

values of R, which is of particular importance for the calculation of the cross second virial coefficient. Similar weighting functions were also used in several of our previous studies (e.g., in Ref. [15]). Note that we quote energies in this work consistently in units of kelvin, i.e., we divide them by Boltzmann's constant k_B but omit k_B from the notation for brevity.

The fit was constrained such that the site charges q in each molecule add up to zero and that the charge distribution reproduces multipole moments (up to octupole) of the two molecules obtained from *ab initio* calculations at the frozen-core CCSD(T) level with the aug-cc-pV6Z [37] basis set using CFOUR [35]. In these calculations, we used again the zero-point vibrationally averaged geometries. The multipole moments are listed in the Supporting Information.

Figure 1 shows the optimized positions of the interaction sites in the two molecules, while Fig. 2 displays the deviations of the fitted interaction energies from the corresponding *ab initio* calculated ones as a function of the latter up to 15,000 K (with the full range of investigated interaction energies extending up to almost 200,000 K for some angular orientations). It can be seen in Fig. 2 that the relative deviations are mostly within ±2%. When calculating thermophysical properties, the fitting errors with positive and negative sign should largely cancel out. We note that the lowest unphysical maximum of the analytical potential function (which is a pure fitting artifact) occurs only at about 71,000 K. This is unproblematic for the thermophysical property calculations of the present work. Wheatley and Harvey [18] considered interaction energies up to about 46,000 K for the fit of their H_2O–CO_2 PES, but the lowest unphysical maximum occurs already at about 4000 K. Since the kinetic theory calculations of the transport properties presented in Section 3.2 involve H_2O–CO_2 interaction energies far in excess of 4000 K, the potential function of Wheatley and Harvey [18] is unsuitable for these calculations. The potential functions of Makarewicz [17] and of Wang and Bowman [19] are even more restricted in their coverage of the highly repulsive regions of the PES because the range of investigated interaction energies was restricted to at most about 3600 K and 4300 K, respectively.

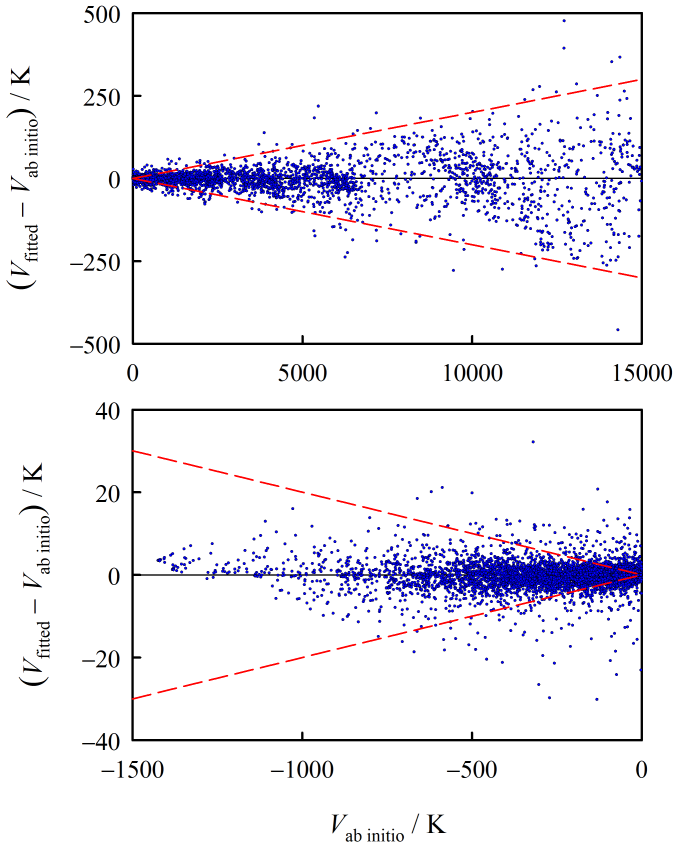

Figure 2: Deviations of interaction energies obtained with the fitted analytical H_2O–CO_2 potential function from the corresponding *ab initio* calculated values as a function of the latter. The dashed lines indicate relative deviations of ±2%.

To give an impression of the shape of the PES, Fig. 3 illustrates the separation dependence of the new analytical potential function in the well region for 12 of the 1012 considered angular orientations. The corresponding *ab initio* calculated interaction energies are also shown in the figure. In agreement with the findings by Makarewicz [17] and by Wang and Bowman [19], the analytical PES features only a single minimum, whose angular orientation corresponds to that indicated by a yellow filled circle. The interaction energy at the minimum, $V_{\text{min}} = -1452.7$ K, is also in good agreement with that found by Makarewicz, $V_{\text{min}} = -1444.5$ K, and that of the PES of Wang and Bowman, $V_{\text{min}} = -1474.5$ K. The minimum of the PES of Wheatley and Harvey [18], $V_{\text{min}} = -1423.5$ K, corresponds to a different angular orientation, which, as discussed in Ref. [18], is a fitting artifact.

The Supporting Information provides further details of the minimum geometry as well as a Fortran 90 implementation of the analytical PES.

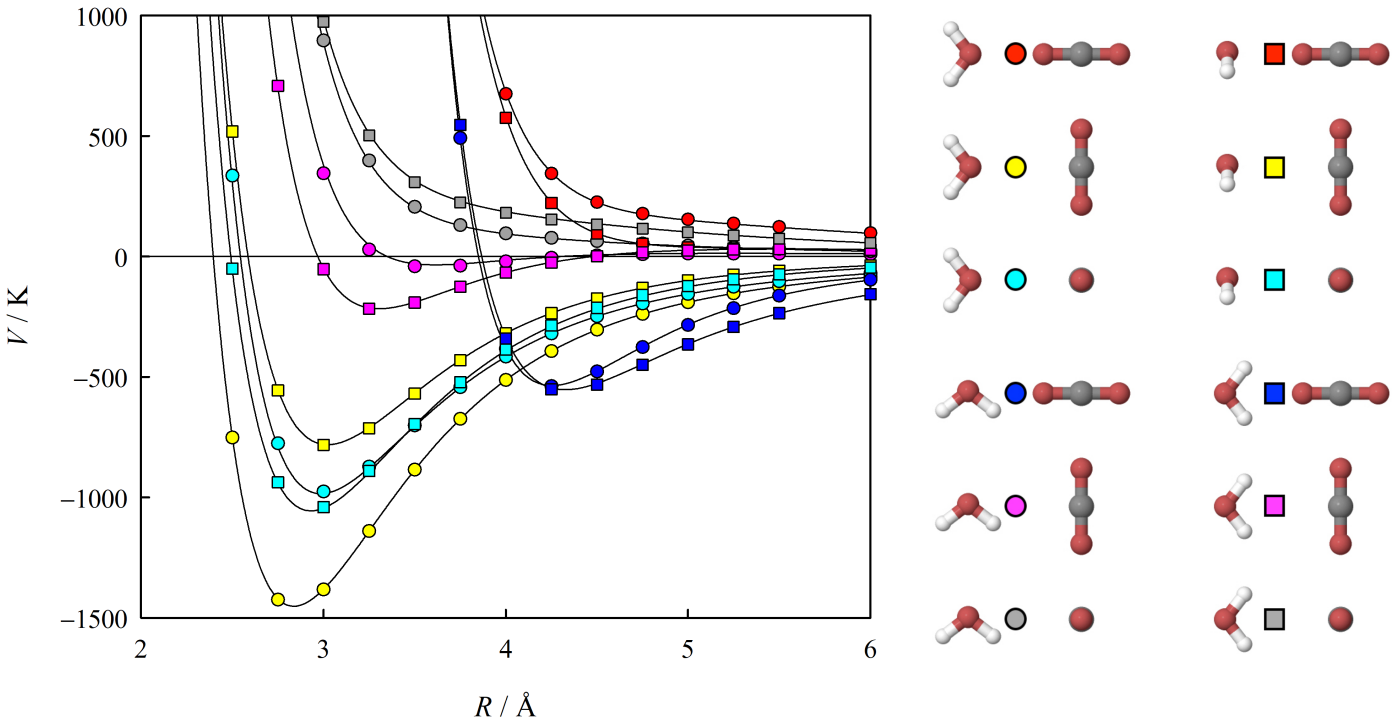

Figure 3: H_2O–CO_2 pair potential as a function of the center-of-mass separation R for 12 of the 1012 considered angular configurations. The symbols represent the *ab initio* calculated values and the solid lines the fitted analytical potential function. The curve representing the orientation indicated by a yellow filled circle passes through the only minimum of the PES.

3. Calculation of thermophysical properties

3.1. Cross second virial coefficient

For two rigid molecules, the classical-mechanical expression for the cross second virial coefficient is

$$B_{12}^{\mathrm{cl}} = -\frac{N_\mathrm{A}}{2}\int_0^\infty \left\langle \exp\left[-\frac{V(\mathbf{R},\Omega_1,\Omega_2)}{k_\mathrm{B}T}\right]-1\right\rangle_{\Omega_1,\Omega_2} \mathrm{d}\mathbf{R}, \quad (6)$$

where N_A is Avogadro's constant, T is the temperature, $\mathbf{R}$ is the separation vector between the centers of mass of the two molecules, Ω_1 and Ω_2 represent the angular orientations of molecules 1 and 2, respectively, and the angle brackets indicate a proper averaging over these orientations. The masses and moments of inertia of the molecules H_2O and CO_2 are large enough to justify accounting for quantum effects semiclassically at all temperatures of interest by replacing the pair potential V in Eq. (6) by the so-called quadratic Feynman–Hibbs (QFH) effective pair potential [38]. For the H_2O–CO_2 pair, it can be written as

$$V_\mathrm{QFH} = V + \frac{\hbar^2}{24k_\mathrm{B}T}\left[\frac{1}{\mu}\left(\frac{\partial^2 V}{\partial x^2}+\frac{\partial^2 V}{\partial y^2}+\frac{\partial^2 V}{\partial z^2}\right)+\frac{1}{I_{1\mathrm{a}}}\frac{\partial^2 V}{\partial \psi_{1\mathrm{a}}^2} + \frac{1}{I_{1\mathrm{b}}}\frac{\partial^2 V}{\partial \psi_{1\mathrm{b}}^2}+\frac{1}{I_{1\mathrm{c}}}\frac{\partial^2 V}{\partial \psi_{1\mathrm{c}}^2}+\frac{1}{I_2}\left(\frac{\partial^2 V}{\partial \psi_{2\mathrm{a}}^2}+\frac{\partial^2 V}{\partial \psi_{2\mathrm{b}}^2}\right)\right], \quad (7)$$

where $\hbar$ is Planck's constant divided by 2π; μ is the reduced mass of the two molecules; x, y, and z are the Cartesian components of $\mathbf{R}$; $I_{1\mathrm{a}}$, $I_{1\mathrm{b}}$, and $I_{1\mathrm{c}}$ denote the three principal moments of inertia of molecule 1 (H_2O); I_2 denotes the moment of inertia of molecule 2 (CO_2) perpendicular to the molecular axis; and the angles $\psi_{1\mathrm{a}}$, $\psi_{1\mathrm{b}}$, $\psi_{1\mathrm{c}}$, $\psi_{2\mathrm{a}}$, and $\psi_{2\mathrm{b}}$ correspond to rotations around the principal axes of the molecules except for the molecular axis of CO_2.

The cross second virial coefficient of the H_2O–CO_2 pair was evaluated for 89 temperatures from (200 to 2000) K using the Mayer-sampling Monte Carlo (MSMC) approach of Singh and Kofke [39]. The hard sphere gas with a sphere diameter of 4.5 Å was employed as the reference system. The results for all temperatures were obtained simultaneously by performing multi-temperature simulations [39, 40], in which the temperature governing the sampling distribution was chosen to be 500 K. To avoid unphysical negative interaction energies at very small intermolecular separations R, hard spheres with a diameter of 1.2 Å were placed on all interaction sites of H_2O and CO_2. In each attempted MSMC move, one of the molecules was displaced and rotated. The maximum step sizes were adjusted during short equilibration runs to yield acceptance rates of 50%. The second derivatives of the pair potential appearing in Eq. (7) were implemented analytically. Values for the cross second virial coefficient from 16 independent simulation runs of 2×10^{10} attempted moves each were averaged. The standard uncertainties of these averages due to the Monte Carlo integration do not exceed 0.012 $\mathrm{cm^3{\cdot}mol^{-1}}$ at any of the investigated temperatures and are hence negligible.

3.2. Dilute gas transport properties

The transport properties of mixtures of molecular gases in the zero-density limit can be calculated with high precision by means of the kinetic theory of molecular gases [7–13, 41–46]. For each transport property, a system of linear equations has to be solved, whose coefficients are given in terms of so-called generalized cross sections. These cross sections are determined by the binary collisions occurring in the gas and are thus directly linked to the intermolecular PESs. The approaches we employed in the present work for the calculation of the shear viscosity η in the third-order kinetic theory approximation, of the thermal conductivity λ (under steady-state conditions, see Ref. [12] for details) in the second-order kinetic theory approximation, and of the product of molar density ρ_m and binary diffusion coefficient D in the third-order kinetic theory approximation from the generalized cross sections were already presented in previous papers [10, 12, 13] and are not repeated here.

Our approach for the calculation of the thermal conductivity [12] requires knowledge of the vibrational contributions to the ideal gas heat capacities of the involved gases. They were extracted from the current reference formulations for the isochoric ideal gas heat capacities [47, 48] by subtracting the translational and classical rotational contributions.

The generalized cross sections for H_2O–CO_2 collisions were determined within the rigid-rotor approximation by means of the proven (see, e.g., Refs. [14, 15, 49]) and highly efficient classical trajectory approach using an extended version of the TRAJECT code [8, 10, 46]. The collision trajectories were obtained by integrating Hamilton's equations from pre- to post-collisional values. A very large initial and final separation of 1000 Å was used to avoid PES cut-off effects. The integration accuracy was chosen such that the relative drift in the total energy between the initial and final state of a trajectory was typically in the range from 10^{-9} to 10^{-6} with a maximum tolerated value of 10^{-4}. Total-energy-dependent generalized cross sections in the center-of-mass frame, which are 11-dimensional integrals over the initial states of the trajectories, were computed from the initial and final states by means of a simple Monte Carlo integration scheme using quasi-random numbers. The calculations were performed for 37 values of the total energy, $E_{total} = E_{trans} + E_{rot}$, which was divided into the three ranges $100 \leqslant E_{total}/K \leqslant 500$, $500 \leqslant E_{total}/K \leqslant 5000$, and $5000 \leqslant E_{total}/K \leqslant 50{,}000$. The 13 energies in each range were chosen as the nodes for Chebyshev interpolation of the cross sections as a function of $\ln(E_{total})$. Up to 2×10^6 trajectories were generated at each total energy value. Below 500 K, the number of trajectories had to be gradually reduced down to 200,000 at 100 K because of the high computational costs of calculating trajectories at very low energies with the desired accuracy. A weighted integration over the total energy (thermal averaging) yielded temperature-dependent generalized cross sections in the center-of-mass frame at temperatures from (250 to 2000) K, which were then converted to the laboratory frame cross sections needed in the systems of linear equations that have to be solved to finally obtain the transport properties.

The generalized cross sections for H_2O–H_2O and CO_2–CO_2 collisions were obtained from high-level *ab initio* pair potentials [3–5] in previous studies [3, 11, 20] in a similar way as described here for the H_2O–CO_2 case.

The relative standard uncertainty of the calculated transport property values due to the above-mentioned Monte Carlo integration scheme is estimated (based on uncertainty estimates generated by TRAJECT for the individual cross sections as described in Ref. [50]) to be less than 0.15% for viscosity and the binary diffusion coefficient and less than 0.3% for thermal conductivity for all temperatures and mole fractions. Errors resulting from the numerical integration of Hamilton's equations and from the Chebyshev interpolation of the total-energy-dependent generalized cross sections and the subsequent thermal averaging should be negligible.

4. Results and discussion

4.1. Cross second virial coefficient

Table 1 lists the classically calculated values, B_{12}^{cl}, and the semiclassically calculated ones, B_{12}^{QFH}, for the H_2O–CO_2 cross second virial coefficient as well as the estimated uncertainties of B_{12}^{QFH} (see below) at 38 selected temperatures. The differences between B_{12}^{cl} and B_{12}^{QFH} decrease, as expected, rapidly with increasing temperature. The classical values deviate from the semiclassical ones by $-73.0\ cm^3{\cdot}mol^{-1}$ at 200 K, $-8.52\ cm^3{\cdot}mol^{-1}$ at 300 K, $-1.19\ cm^3{\cdot}mol^{-1}$ at 500 K, and $-0.03\ cm^3{\cdot}mol^{-1}$ at 2000 K.

In Fig. 4, the calculated values are compared with most of the available experimental data [18, 51–59], which unfortunately exhibit a large scatter. However, the data of Patel et al. [56] stand out due to their excellent agreement (within $\pm 2\ cm^3{\cdot}mol^{-1}$ apart from one datum) with the calculated values. Furthermore, the recent data by Meyer and Harvey [59] agree very well with the calculated values. Only their datum at the lowest temperature exhibits larger positive deviations. However, it should be pointed out that the virial analysis performed by Meyer and Harvey at this temperature yielded a distinctly too negative H_2O–CO_2–CO_2 cross third virial coefficient as can be seen in Fig. 8 of Ref. [60], indicating that the derived value for the cross second virial coefficient is too high to compensate for this. Figure 4 also shows values calculated semiclassically by Schultz et al. [60] using the PES of Wheatley and Harvey [18] as well as the correlation of Wheatley and Harvey [61], which was fitted to semiclassical values that Wheatley and Harvey obtained from their PES independently of Schultz et al. The small systematic differences between the values of Schultz et al. and the correlation of Wheatley and Harvey at the lowest temperatures are probably caused by the use of slightly different semiclassical approaches. At most temperatures, the cross second virial coefficients obtained with the PES of Wheatley and Harvey show negative deviations from the present results, but the deviations are within the mutual uncertainties. If one discards the data points at room temperature of King and Coan [51], Wormald and Colling [52], Vanderzee and Haas [53], Wormald et al. [54], and Smith and Wormald [55], which are undoubtedly significantly too negative, it becomes clear that the new PES of the present work yields values that are overall in better

Table 1: Classically calculated values, B_{12}^{cl}, and semiclassically calculated values, B_{12}^{QFH}, of the H_2O–CO_2 cross second virial coefficient as well as the estimated combined expanded uncertainty ($k = 2$) of the semiclassical values, $U\left(B_{12}^{\mathrm{QFH}}\right)$, as a function of temperature T.

T/K	$B_{12}^{\mathrm{cl}}/\mathrm{cm^3{\cdot}mol^{-1}}$	$B_{12}^{\mathrm{QFH}}/\mathrm{cm^3{\cdot}mol^{-1}}$	$U\left(B_{12}^{\mathrm{QFH}}\right)/\mathrm{cm^3{\cdot}mol^{-1}}$
200	−734.3	−661.3	39.7
220	−505.5	−464.4	27.9
240	−371.8	−346.4	20.8
260	−286.5	−269.7	16.2
280	−228.4	−216.7	13.0
300	−186.7	−178.1	10.7
320	−155.5	−149.1	8.9
340	−131.5	−126.6	7.6
360	−112.5	−108.6	6.5
380	−97.16	−93.97	5.6
400	−84.50	−81.88	4.9
420	−73.91	−71.72	4.3
440	−64.93	−63.08	3.8
460	−57.23	−55.65	3.3
480	−50.56	−49.20	3.0
500	−44.74	−43.55	3.0
520	−39.61	−38.57	3.0
540	−35.07	−34.15	3.0
560	−31.02	−30.20	3.0
580	−27.38	−26.65	3.0
600	−24.10	−23.45	3.0
620	−21.14	−20.54	3.0
640	−18.44	−17.90	3.0
660	−15.98	−15.49	3.0
680	−13.72	−13.27	3.0
700	−11.65	−11.24	3.0
750	−7.14	−6.80	3.0
800	−3.41	−3.12	3.0
850	−0.27	−0.03	3.0
900	2.40	2.60	3.0
950	4.69	4.87	3.0
1000	6.68	6.83	3.0
1100	9.93	10.05	3.0
1200	12.48	12.57	3.0
1400	16.15	16.22	3.0
1600	18.63	18.68	3.0
1800	20.38	20.41	3.0
2000	21.64	21.67	3.0

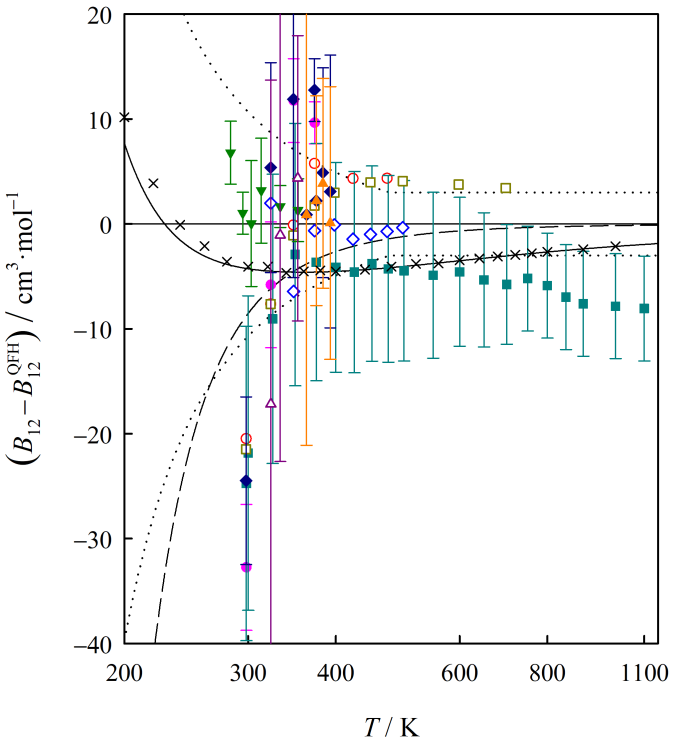

Figure 4: Deviations of experimental data and calculated values for the H_2O–CO_2 cross second virial coefficient from values calculated semiclassically using the H_2O–CO_2 PES of the present work as a function of temperature: ●, King and Coan [51]; ○, Wormald and Colling [52]; ■, Vanderzee and Haas [53]; □, Wormald et al. [54]; ◆, Smith and Wormald [55]; ◇, Patel et al. [56]; ▲, Wormald and Lancaster [57]; △, Bamberger et al. [58] (derived from their phase-equilibrium data by Wheatley and Harvey [18]); ▼, Meyer and Harvey [59]; ×, Schultz et al. [60] (semiclassically calculated values using the PES of Wheatley and Harvey [18]); solid line, correlation by Wheatley and Harvey [61] (fitted to values calculated semiclassically using their PES); dashed line, B_{12}^{cl}; dotted lines, $B_{12}^{\mathrm{QFH}} \pm U\left(B_{12}^{\mathrm{QFH}}\right)$ with $k = 2$.

agreement with the experimental data than those resulting from the PES of Wheatley and Harvey.

The B_{12} values from the Wormald group [52, 54, 55, 57] were derived from measurements of the enthalpy of mixing of the two gases at low density. The quantity that is actually more directly related to such data is the dilute gas cross isothermal Joule–Thomson coefficient $\phi_{12} = B_{12} - T(\mathrm{d}B_{12}/\mathrm{d}T)$. Values for ϕ_{12} are only given in two of the four papers [55, 57], and the other papers unfortunately do not provide sufficient information to determine them. However, Wheatley and Harvey [61] were able to derive ϕ_{12} values from enthalpy of mixing data given by Lancaster and Wormald [62]. In Fig. 5, the experimental ϕ_{12} values and those resulting from the correlation for B_{12} by Wheatley and Harvey [61] are compared with the values obtained from a correlation of the present B_{12}^{QFH} values (see Section 5). While the agreement of the two correlations with the data by Smith and Wormald [55] and by Wormald and Lancaster [57] (with the latter resulting from a re-evaluation of the former) is poor, the agreement with the ϕ_{12} values derived by Wheatley and Harvey from the enthalpy of mixing data of Lancaster and Wormald is more satisfactory and slightly better for the present correlation than for that by Wheatley and Harvey.

Based on the agreement with the experimental data and on our experience, we estimate the combined expanded uncertainty (coverage factor $k = 2$, corresponding approximately to a 95% confidence level) of the present B_{12}^{QFH} values as the larger of 6% of the absolute value of B_{12}^{QFH} and 3 cm^3·mol^{-1}. This estimate is also indicated in Fig. 4. The largest error source is most likely the treatment of the molecules as rigid rotors; see also the recent study by Garberoglio et al. [63] on the effect of monomer flexibility on the second and third virial coefficients of normal and heavy water. Other error sources are the semiclassical treatment of quantum effects, the approximate nature of the employed quantum-chemical approaches, and the fitting errors of the analytical potential function. Note that partial thermal decomposition of real H_2O and CO_2 molecules at the highest investigated temperatures is not taken into account for any of the uncertainty estimates provided in this work.

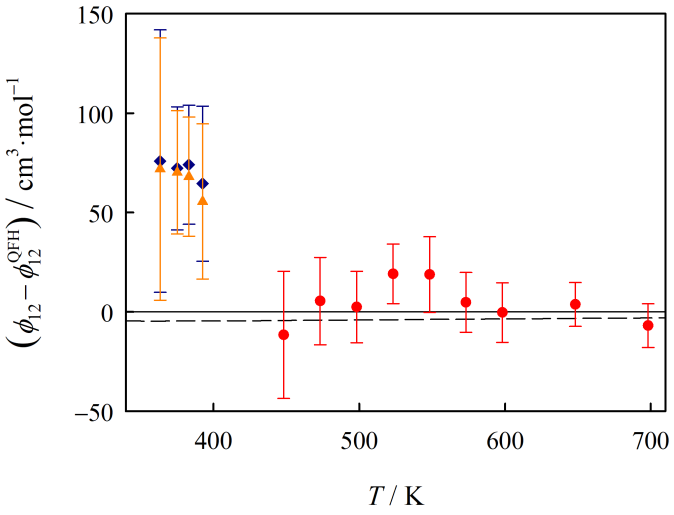

Figure 5: Deviations of experimental data and calculated values of the dilute gas cross isothermal Joule–Thomson coefficient $\phi_{12} = B_{12} - T(\mathrm{d}B_{12}/\mathrm{d}T)$ for the H_2O–CO_2 interaction from the respective values derived from a correlation of the B_{12}^{QFH} values of the present work as a function of temperature: ◆, Smith and Wormald [55]; ▲, Wormald and Lancaster [57]; ●, Lancaster and Wormald [62] (derived from their enthalpy of mixing data by Wheatley and Harvey [18]); dashed line, values calculated using the correlation for B_{12} by Wheatley and Harvey [61].

4.2. *Dilute gas transport properties*

Tables 2 and 3 list the calculated values for the dilute gas shear viscosity η and thermal conductivity λ, respectively, of (H_2O + CO_2) mixtures for 26 temperatures from (250 to 2000) K and nine mole fractions x_{H_2O}. The values for the pure components, which were obtained in previous studies [3, 11, 20], are also listed there. Table 4 provides the calculated values for the dilute gas limit of the product of molar density ρ_m and binary diffusion coefficient D for the same 26 temperatures and for five mole fractions.

The $\eta(T, x_{H_2O})$ and $\lambda(T, x_{H_2O})$ surfaces are visualized in Fig. 6. The figure reveals non-trivial mole fraction dependences, with maxima occurring for $x_{H_2O} \neq 0$ and $x_{H_2O} \neq 1$ above about 710 K for η and below about 810 K for λ and with the latter quantity exhibiting a change in curvature from concave up to about 1430 K to convex above that temperature.

The variation of $\rho_m D$ with mole fraction is small and monotonic as can be seen in Table 4; it does not exceed 1.63% at any temperature. However, this is not unexpected as the mole fraction dependence of $\rho_m D$ is a higher-order kinetic theory effect. In the first-order kinetic theory approximation, $\rho_m D$ is independent of mole fraction and determined entirely by the unlike interactions, i.e., the H_2O–CO_2 PES.

The relative influence of the order of the kinetic theory on the calculated values for all three transport properties is visualized in the form of ratios in Fig. 7, which shows that the viscosity converges much more rapidly with increasing order than the binary diffusion coefficient and is essentially converged for the third-order theory. The neglect of fourth- and higher-order contributions to the binary diffusion coefficient can be expected to introduce errors of less than 0.1%. For the thermal conductivity, for which we did not investigate a third-order approximation, the second-order contribution is quite large, exceeding 2% for CO_2-rich mixtures at higher temperatures. This is due to the large effect of angular momentum polarization on the thermal conductivity of CO_2 [64], which is not accounted for in the first-order theory, but should be almost fully included at the second-order level. The other effects that determine the magnitude of the higher-order kinetic theory contributions to the thermal conductivity should show a convergence behavior similar to that for monatomic gas mixtures, which is as slow as that for the binary diffusion coefficient [65]. Thus, for the (H_2O + CO_2) system the convergence behavior for the thermal conductivity should be in between that for viscosity and that for binary diffusion, and we estimate the errors resulting from the neglect of third- and higher-order contributions to be at most 0.2%.

Experimental information on the viscosity of (H_2O + CO_2) mixtures is virtually non-existent. The only data are those of Munczak and Sedlacek [66], who measured the change in viscosity of CO_2 at 303 K resulting from adding small amounts of water vapor up to a mole fraction of $x_{H_2O} = 0.038$. As illustrated in Fig. 8, their data exhibit a slight downward trend with increasing water mole fraction, but it is not as pronounced as for the calculated values.

As in our studies on the mixtures (CH_4 + N_2) [10], (CH_4 + CO_2) [13], (CH_4 + H_2S) [13], (H_2S + CO_2) [13], (CH_4 + C_3H_8) [14], (CO_2 + C_3H_8) [14], (CO_2 + N_2) [15], and (H_2S + N_2) [16], we propose a simple scaling of the calculated viscosity values by a temperature-independent factor that depends linearly on the mole fraction to obtain values with the lowest possible uncertainty,

$$\eta_{rec} = \eta_{calc}\,(1.001 x_{H_2O} + 1.0055 x_{CO_2})\,, \qquad (8)$$

where η_{rec} and η_{calc} are the recommended and calculated viscosity values, respectively. The scaling factors 1.001 and 1.0055 correspond to those proposed previously for H_2O [20] and CO_2 [3], respectively, and remedy systematic deviations of the calculated viscosity values from the best available experimental data.

Figure 9 shows the comparison of the calculated thermal conductivity values with the three available data sets for the mixture [67–69]. The data of Timrot and Vargaftik [67] were measured at (338 and 603) K by the hot-wire method. They exhibit mostly positive deviations up to 3.9%, but capture the mole fraction dependence of the calculated values quite well. Dijkema et al. [68] measured the thermal conductivity at (298 and 333) K by the hot-wire method and a thermistor katharometer bridge. The deviations of their data vary smoothly with mole fraction between the pure components and amount to at most −4.3%. The most recent dilute gas data are those of Perkins [69] for temperatures from (503 to 622) K. He obtained them from thermal conductivity data that he measured with the hot-wire method by extrapolation down to atmospheric pressure. His data agree very well, mostly within the experimental uncertainty, with the calculated values over the whole composition range.

For the thermal conductivity of pure CO_2, there exists a remarkably accurate data set for temperatures from (328 to

Table 2: Calculated values for the dilute gas shear viscosity η of mixtures of H_2O (1) and CO_2 (2) as a function of mole fraction x_1 and temperature T. Previously calculated viscosities for pure H_2O [20] and pure CO_2 [3] are also listed here.[a]

T/K	η/μPa·s										
	$x_1 = 0$	$x_1 = 0.1$	$x_1 = 0.2$	$x_1 = 0.3$	$x_1 = 0.4$	$x_1 = 0.5$	$x_1 = 0.6$	$x_1 = 0.7$	$x_1 = 0.8$	$x_1 = 0.9$	$x_1 = 1$
250	12.51	12.32	12.09	11.80	11.46	11.06	10.60	10.07	9.473	8.802	8.054
273.15	13.63	13.44	13.20	12.90	12.54	12.11	11.61	11.03	10.38	9.645	8.819
298.15	14.82	14.64	14.39	14.08	13.70	13.24	12.71	12.09	11.38	10.57	9.660
330	16.32	16.14	15.90	15.57	15.18	14.69	14.11	13.44	12.66	11.77	10.76
360	17.71	17.54	17.29	16.97	16.56	16.05	15.44	14.73	13.89	12.93	11.83
400	19.52	19.36	19.12	18.80	18.38	17.86	17.22	16.45	15.55	14.51	13.31
450	21.69	21.56	21.34	21.03	20.61	20.08	19.42	18.61	17.66	16.54	15.23
500	23.78	23.67	23.48	23.18	22.78	22.25	21.58	20.77	19.78	18.61	17.24
550	25.79	25.70	25.53	25.26	24.88	24.37	23.71	22.90	21.91	20.71	19.29
600	27.71	27.66	27.51	27.27	26.91	26.43	25.80	25.00	24.01	22.82	21.38
650	29.56	29.54	29.42	29.21	28.88	28.43	27.83	27.06	26.10	24.92	23.49
700	31.35	31.35	31.26	31.08	30.79	30.37	29.80	29.07	28.15	27.00	25.60
750	33.07	33.09	33.04	32.89	32.63	32.25	31.73	31.04	30.15	29.05	27.69
800	34.74	34.79	34.76	34.64	34.42	34.07	33.59	32.95	32.12	31.07	29.75
900	37.93	38.02	38.04	37.98	37.83	37.57	37.18	36.64	35.91	34.97	33.78
1000	40.95	41.08	41.14	41.14	41.06	40.87	40.57	40.13	39.52	38.71	37.65
1100	43.83	43.99	44.10	44.15	44.13	44.02	43.80	43.45	42.95	42.26	41.35
1200	46.58	46.78	46.93	47.03	47.06	47.02	46.88	46.62	46.23	45.66	44.87
1300	49.23	49.46	49.65	49.79	49.88	49.90	49.83	49.66	49.36	48.90	48.24
1400	51.79	52.04	52.27	52.46	52.59	52.67	52.67	52.58	52.37	52.01	51.47
1500	54.27	54.55	54.81	55.03	55.22	55.35	55.41	55.39	55.26	55.00	54.57
1600	56.67	56.99	57.28	57.54	57.76	57.94	58.06	58.11	58.06	57.88	57.56
1700	59.02	59.35	59.67	59.97	60.24	60.47	60.64	60.75	60.77	60.67	60.44
1800	61.30	61.67	62.02	62.35	62.65	62.92	63.15	63.31	63.40	63.38	63.24
1900	63.54	63.93	64.31	64.67	65.01	65.32	65.60	65.81	65.96	66.02	65.95
2000	65.72	66.14	66.54	66.94	67.32	67.67	67.99	68.26	68.47	68.59	68.59

[a] The viscosity values should be scaled using Eq. (8) to obtain the recommended values. The relative combined expanded uncertainty ($k = 2$) of the scaled values for the mixtures is estimated to be 1.0% from (300 to 500) K and 2.0% otherwise. The respective estimate for the scaled viscosities of pure H_2O is 0.4% from (300 to 500) K, 0.8% below 300 K, and 2.0% above 500 K [20], and that for the scaled viscosities of pure CO_2 is 0.4% from (300 to 700) K and 2.0% otherwise [15].

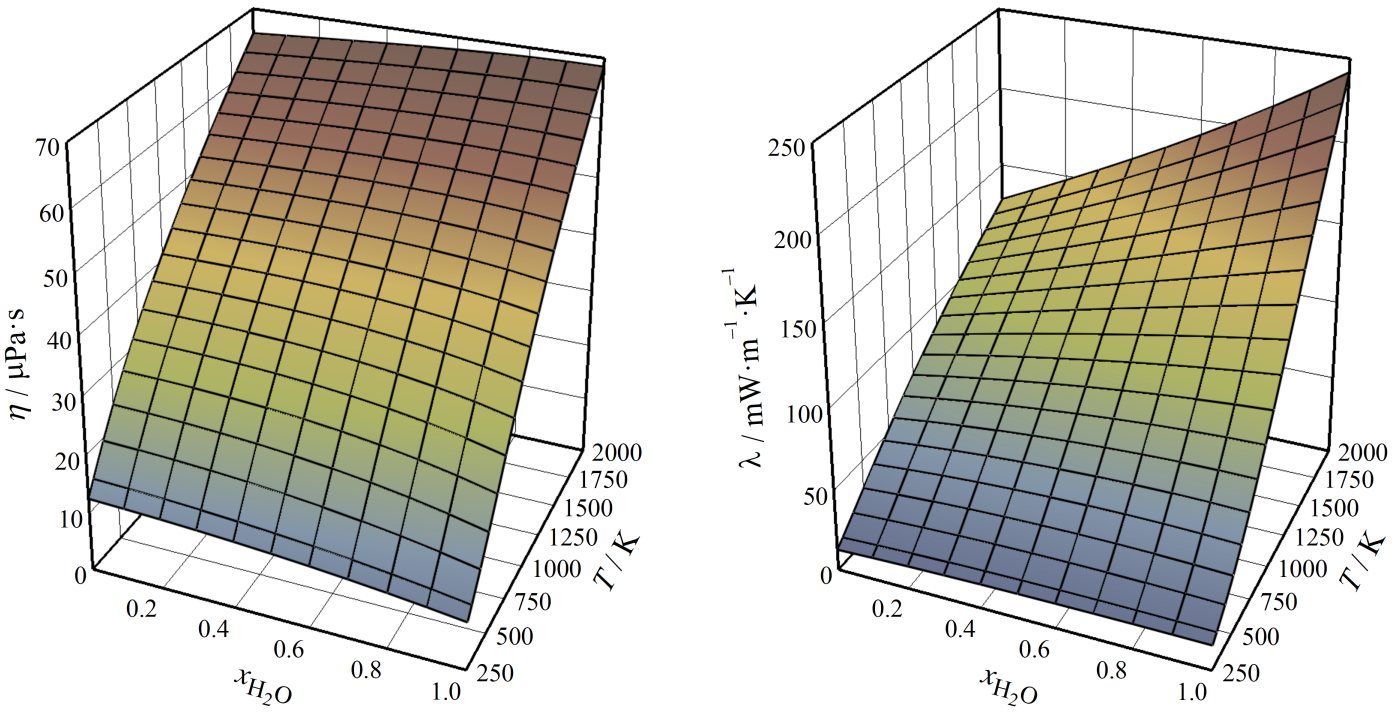

Figure 6: Calculated dilute gas viscosity (left) and thermal conductivity (right) of the (H_2O + CO_2) system as a function of water vapor mole fraction and temperature.

Table 3: Calculated values for the dilute gas thermal conductivity λ of mixtures of H_2O (1) and CO_2 (2) as a function of mole fraction x_1 and temperature T. Previously calculated thermal conductivities for pure H_2O [11] and pure CO_2 [3] are also listed here.[a]

T/K	λ/mW·m^{-1}·K^{-1}										
	$x_1 = 0$	$x_1 = 0.1$	$x_1 = 0.2$	$x_1 = 0.3$	$x_1 = 0.4$	$x_1 = 0.5$	$x_1 = 0.6$	$x_1 = 0.7$	$x_1 = 0.8$	$x_1 = 0.9$	$x_1 = 1$
250	12.77	13.49	14.06	14.50	14.83	15.06	15.22	15.30	15.30	15.24	15.12
273.15	14.44	15.22	15.82	16.29	16.63	16.86	17.00	17.05	17.01	16.89	16.69
298.15	16.31	17.15	17.80	18.29	18.64	18.88	18.99	19.01	18.92	18.73	18.45
330	18.77	19.69	20.40	20.94	21.31	21.54	21.64	21.61	21.46	21.19	20.79
360	21.15	22.15	22.92	23.50	23.90	24.14	24.23	24.17	23.96	23.61	23.11
400	24.36	25.49	26.36	27.01	27.46	27.73	27.81	27.73	27.46	27.02	26.39
450	28.42	29.71	30.72	31.49	32.03	32.36	32.48	32.39	32.09	31.57	30.82
500	32.49	33.96	35.13	36.03	36.69	37.11	37.30	37.25	36.96	36.42	35.59
550	36.53	38.19	39.54	40.61	41.41	41.96	42.26	42.29	42.05	41.53	40.69
600	40.54	42.40	43.94	45.19	46.17	46.87	47.31	47.47	47.33	46.88	46.08
650	44.48	46.56	48.31	49.76	50.93	51.83	52.44	52.76	52.77	52.45	51.75
700	48.37	50.67	52.64	54.32	55.70	56.81	57.63	58.15	58.35	58.20	57.67
750	52.19	54.72	56.93	58.84	60.47	61.81	62.87	63.63	64.06	64.14	63.81
800	55.93	58.71	61.17	63.33	65.21	66.82	68.15	69.17	69.88	70.23	70.17
900	63.20	66.49	69.48	72.19	74.65	76.85	78.78	80.44	81.80	82.81	83.43
1000	70.15	73.99	77.56	80.88	83.98	86.84	89.48	91.87	94.00	95.82	97.29
1100	76.82	81.24	85.42	89.39	93.17	96.77	100.2	103.4	106.4	109.1	111.6
1200	83.21	88.23	93.05	97.71	102.2	106.6	110.8	114.9	118.9	122.6	126.2
1300	89.36	94.99	100.5	105.8	111.1	116.3	121.4	126.4	131.4	136.2	140.9
1400	95.27	101.5	107.7	113.8	119.8	125.8	131.8	137.8	143.8	149.8	155.7
1500	101.0	107.9	114.7	121.5	128.3	135.2	142.1	149.0	156.1	163.3	170.5
1600	106.5	114.0	121.5	129.0	136.6	144.3	152.2	160.1	168.3	176.6	185.1
1700	111.9	120.0	128.2	136.4	144.8	153.3	162.1	171.0	180.3	189.8	199.6
1800	117.1	125.8	134.6	143.6	152.8	162.2	171.8	181.8	192.1	202.8	213.9
1900	122.1	131.5	141.0	150.6	160.6	170.8	181.4	192.3	203.7	215.6	228.1
2000	127.1	137.0	147.2	157.5	168.2	179.3	190.7	202.7	215.1	228.2	242.0

[a] The thermal conductivity values should be scaled using Eq. (9) to obtain the recommended values. The relative combined expanded uncertainty ($k = 2$) of the scaled values for the mixtures is estimated to be the same as that for pure CO_2, namely 2% from (300 to 700) K and 4% otherwise [15]. The respective uncertainty of the thermal conductivity values for pure H_2O is assessed here to be 2% from (250 to 1000) K and 3% above 1000 K.

468) K, measured by Haarman [70] using a transient hot-wire apparatus. These data have a stated uncertainty of 0.3% and are included in Fig. 9 to illustrate the accuracy of the calculated thermal conductivity values for CO_2, which are on average only 1.1% smaller.

To remedy the systematic deviations from the data of Haarman [70], we also propose a scaling of the calculated thermal conductivity values,

$$\lambda_{\mathrm{rec}} = \lambda_{\mathrm{calc}} \left(x_{\mathrm{H_2O}} + 1.011 x_{\mathrm{CO_2}} \right) . \qquad (9)$$

We recommended such a scaling previously for pure CO_2 [3] and for the mixtures $(CH_4 + CO_2)$ [13], $(H_2S + CO_2)$ [13], $(CO_2 + C_3H_8)$ [14], and $(CO_2 + N_2)$ [15]. A scaling for H_2O is not recommended because there are no apparent systematic deviations from the best experimental data (see Fig. 1 of Ref. [11]).

In Fig. 10, we compare the calculated values for the product of molar density and binary diffusion coefficient with the available experimental data [71–77]. Apart from two data points that are obvious outliers, the agreement is within ±5.4%. If we consider only the data of Winkelmann [72], their re-evaluation by Trautz and Müller [73], the data of Rossié [75], and those of Nagata and Hasegawa [77], the agreement is even within ±2.9%. None of the experimental papers provides information on the mole fraction composition of the mixtures or even their influence on the diffusion coefficient, although it would be possible to put constraints on the composition in some of the low-temperature experiments by taking into account that the partial pressure of H_2O in the gas mixture cannot exceed the saturated vapor pressure. However, since the uncertainties of the experimental data are obviously much larger than the mole fraction dependence, we simply assumed equimolar mixtures for the calculation of the deviations from our calculated values.

Estimates of the relative combined expanded uncertainties ($k = 2$) of the calculated values for the binary diffusion coefficient and of the scaled viscosity and thermal conductivity values are provided in the footnotes of Tables 2–4. These estimates are based mainly on experience. As in the case of the cross second virial coefficient, the largest source of uncertainty is probably the treatment of the molecules as rigid rotors. At low temperatures, one might expect that the classical-mechanical calculation of the generalized cross sections causes sizable errors. However, the calculated viscosity and thermal conductivity values for the pure components [3, 11, 20] do not exhibit increasing systematic deviations from the best experimental data toward the lowest temperatures that could be interpreted as being caused by the neglect of quantum effects.

5. Correlations

A practical correlation for the cross second virial coefficient was obtained by fitting a polynomial in $(T^*)^{-1/2}$ with

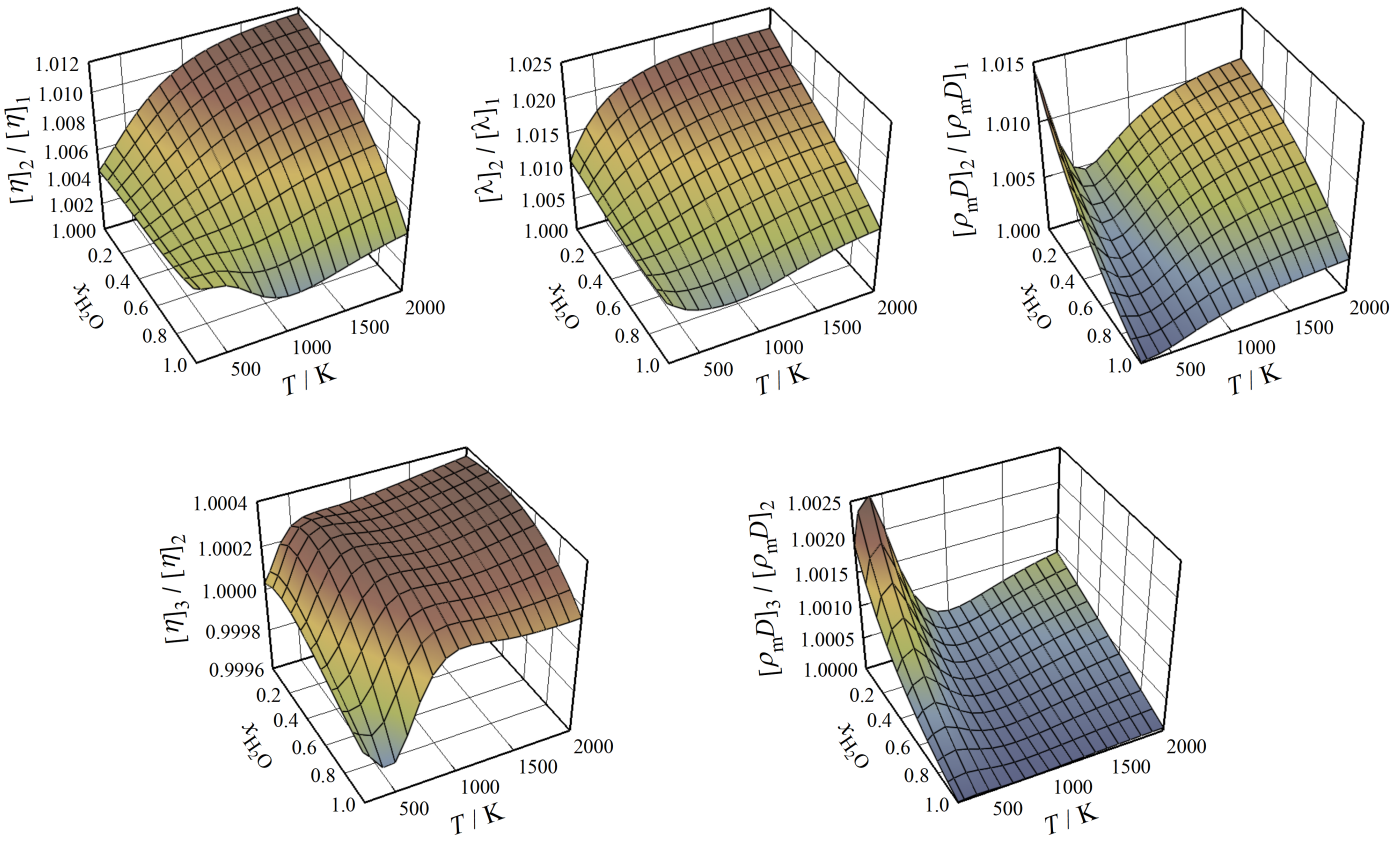

Figure 7: Ratios of dilute gas transport property values for the (H_2O + CO_2) system resulting from different orders of kinetic theory approximations as a function of water vapor mole fraction and temperature. The nth-order approximation of a transport property X (with $X \in \{\eta, \lambda, \rho_m D\}$) is denoted here as $[X]_n$.

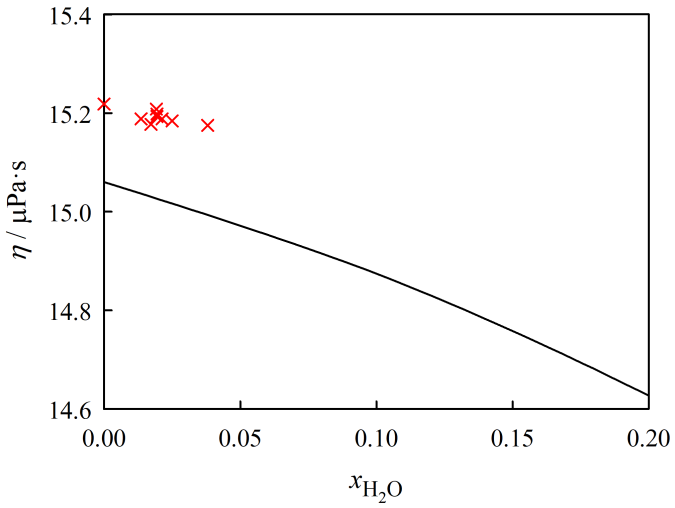

Figure 8: Experimental data of Munczak and Sedlacek [66] (×) for the dilute gas viscosity of the (H_2O + CO_2) system at 303 K and calculated values of the present work for the same temperature (solid line) as a function of water vapor mole fraction.

$T^* = T/(100\ \mathrm{K})$ to the 89 calculated values for B_{12}^{QFH}. The symbolic regression software Eureqa (version 1.24.0) [78] was employed to find an optimal polynomial structure. The resulting expression is

$$\frac{B_{12}^{\mathrm{QFH}}}{\mathrm{cm^3 \cdot mol^{-1}}} = b_1 + \frac{b_2}{(T^*)^{1/2}} + \frac{b_3}{T^*} + \frac{b_4}{(T^*)^3} + \frac{b_5}{(T^*)^6} + \frac{b_6}{(T^*)^{21/2}}, \tag{10}$$

where $b_1 = 15.244$, $b_2 = 149.51$, $b_3 = -534.35$, $b_4 = -2243.2$, $b_5 = -1.3200 \times 10^4$, and $b_6 = -4.1246 \times 10^4$. Equation (10) reproduces the calculated values within ± 0.007 cm^3·mol^{-1} and extrapolates reasonably to temperatures below 200 K and above 2000 K as shown in Fig. 11. It is interesting to note that the structure of Eq. (10) is identical to that obtained previously for the correlation of the second virial coefficient of ethane [49].

A correlation for $\rho_m D$ was developed based on the calculated values of the present work for temperatures from (250 to 2000) K in the same manner as previously for the (CO_2 + N_2) [15] and (H_2S + N_2) [16] systems. For convenience, the small composition dependence of $\rho_m D$ was neglected and the correlation fitted to the values for an equimolar mixture. The basic form of the correlation is

$$\frac{10^4 \times \rho_m D}{\mathrm{mol \cdot m^{-1} \cdot s^{-1}}} = \frac{\overline{T}^{1/2}}{S(\overline{T})}, \tag{11}$$

where $\overline{T} = T/\mathrm{K}$. If $\rho_m D$ were to be obtained using the first-order kinetic theory approximation, $S(\overline{T})$ would be proportional to a single generalized cross section, which decreases monotonically with temperature. To find a functional form for $S(\overline{T})$ that

Table 4: Calculated values for the product of molar density ρ_m and binary diffusion coefficient D of mixtures of H_2O (1) and CO_2 (2) in the dilute gas limit as a function of mole fraction x_1 and temperature T.[a]

T/K	$10^4 \times \rho_m D$/mol·m^{-1}·s^{-1}				
	$x_1 \to 0$	$x_1 = 0.2$	$x_1 = 0.5$	$x_1 = 0.8$	$x_1 \to 1$
250	5.472	5.442	5.413	5.394	5.384
273.15	6.066	6.035	6.004	5.983	5.973
298.15	6.712	6.679	6.647	6.626	6.615
330	7.533	7.500	7.468	7.446	7.435
360	8.299	8.267	8.235	8.214	8.203
400	9.302	9.272	9.242	9.221	9.211
450	10.52	10.49	10.46	10.44	10.44
500	11.69	11.67	11.64	11.62	11.61
550	12.81	12.79	12.77	12.75	12.74
600	13.89	13.87	13.85	13.83	13.82
650	14.93	14.91	14.89	14.87	14.86
700	15.93	15.91	15.89	15.87	15.85
750	16.89	16.87	16.85	16.83	16.81
800	17.82	17.80	17.78	17.75	17.73
900	19.59	19.58	19.55	19.51	19.49
1000	21.27	21.25	21.22	21.18	21.14
1100	22.86	22.84	22.81	22.76	22.72
1200	24.39	24.37	24.33	24.27	24.22
1300	25.86	25.83	25.79	25.73	25.67
1400	27.28	27.25	27.20	27.14	27.07
1500	28.65	28.63	28.57	28.50	28.43
1600	29.99	29.96	29.91	29.83	29.75
1700	31.30	31.27	31.21	31.12	31.04
1800	32.57	32.54	32.48	32.39	32.31
1900	33.82	33.79	33.72	33.63	33.54
2000	35.04	35.01	34.94	34.84	34.75

[a] The relative combined expanded uncertainty ($k = 2$) of the $\rho_m D$ values is estimated to be 2% from (300 to 700) K and 3% otherwise.

obeys this constraint, while being both accurate and simple, the Eureqa software was again utilized. Following the approach used in our previous work [15, 16], $\overline{T}$ was restricted to appear solely in integer powers of $\overline{T}^{1/6}$. Furthermore, only constants, exponential functions, and the operators addition, subtraction, multiplication, division, and negation were allowed. Of the functions found by Eureqa, the following one best fulfills the requirements:

$$S(\overline{T}) = d_1 + d_2\overline{T}^{-1/6} + d_3\overline{T}^{1/3}\exp\left(-\overline{T}^{1/3}\right) + d_4\exp\left(-2\overline{T}^{1/3}\right) + d_5\exp\left(-3\overline{T}^{1/3}\right), \quad (12)$$

where $d_1 = -0.09647$, $d_2 = 4.8695$, $d_3 = 103.70$, $d_4 = -4.0400 \times 10^4$, and $d_5 = 2.1764 \times 10^6$. The correlation reproduces the calculated $\rho_m D$ values within ±0.01% and extrapolates in a physically reasonable manner to temperatures far above 2000 K and down to about 100 K as illustrated in Fig. 12.

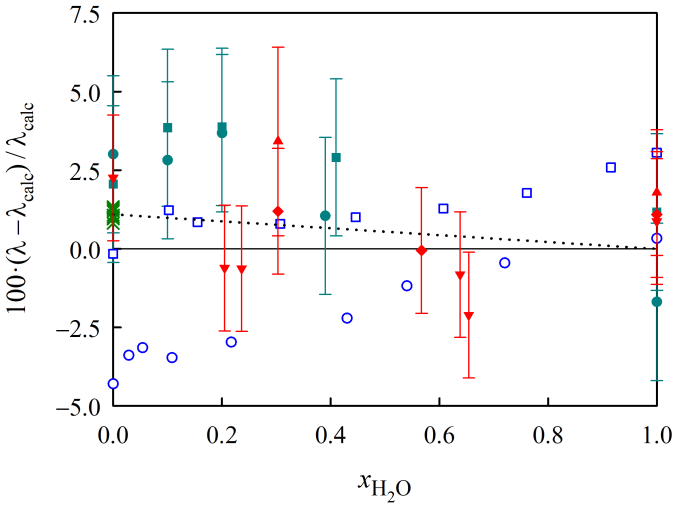

Figure 9: Relative deviations of experimental data for the dilute gas thermal conductivity of the ($H_2O + CO_2$) system from the calculated values of the present work as a function of water vapor mole fraction: ●, Timrot and Vargaftik [67], 338 K; ■, Timrot and Vargaftik [67], 603 K; ○, Dijkema et al. [68], 298 K; □, Dijkema et al. [68], 333 K; ×, Haarman [70], (328 to 468) K; ▼, Perkins [69], (503 to 505) K; ◆, Perkins [69], (562 to 564) K; ▲, Perkins [69], (621 and 622) K; dotted line, recommended values resulting from Eq. (9). For clarity of the figure, the stated uncertainties for the data of Haarman [70] (0.3%) are not indicated by error bars. The data of Timrot and Vargaftik [67] were not published in numerical form and had to be read from their Fig. 7 with an accuracy of about 0.5%, which is taken into account in the displayed error bars.

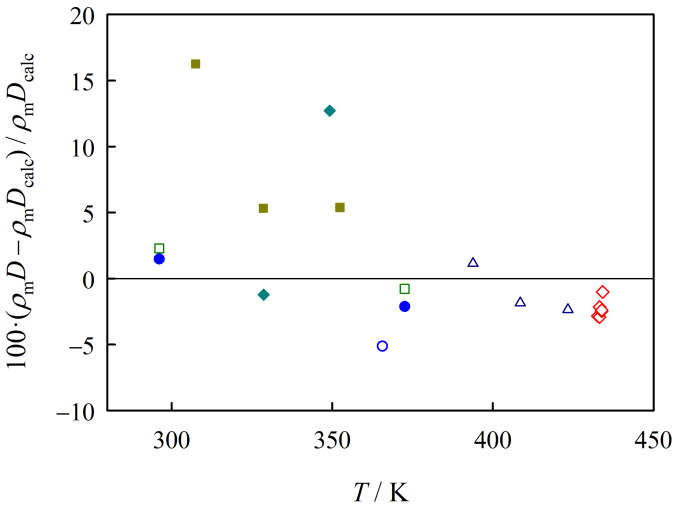

Figure 10: Relative deviations of experimental data for the product of molar density and binary diffusion coefficient of the ($H_2O + CO_2$) system in the dilute gas phase from the calculated values of the present work as a function of temperature: ○, Winkelmann [71]; ●, Winkelmann [72]; □, Trautz and Müller [73] (re-evaluation of the measurements of Winkelmann [72]); ■, Schwertz and Brow [74]; ◇, Rossié [75]; ◆, Crider [76]; △, Nagata and Hasegawa [77].

6. Conclusions

The cross second virial coefficient of the ($H_2O + CO_2$) system and three of its transport properties (shear viscosity, thermal conductivity, and binary diffusion coefficient) in the dilute gas limit were determined with high accuracy at temperatures up to 2000 K applying statistical thermodynamics and the kinetic theory of molecular gases [7–13, 41–46], respectively. The required pair PES for the H_2O–CO_2 interaction was developed as part of the present work employing quantum-chemical *ab initio* computations at the RI-MP2 [23, 24] and the CCSD(T) [33] level of theory for more than 22,000 mutual con-

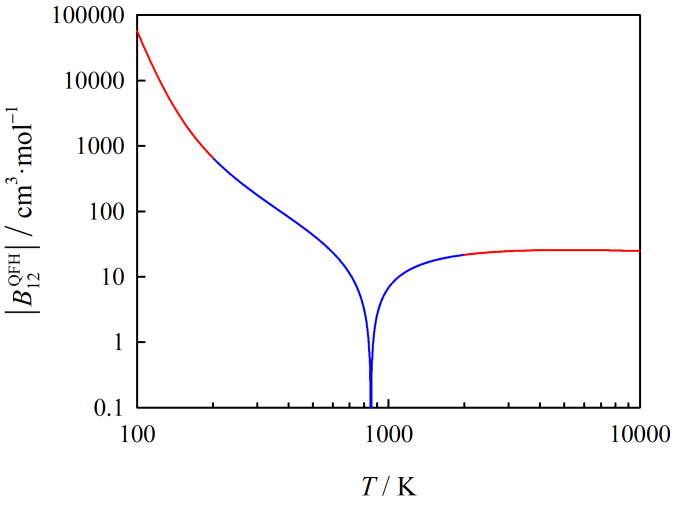

Figure 11: Correlation for the cross second virial coefficient as given by Eq. (10), displayed here as the absolute value. The correlation is colored in blue within its range of validity and in red outside of this range.

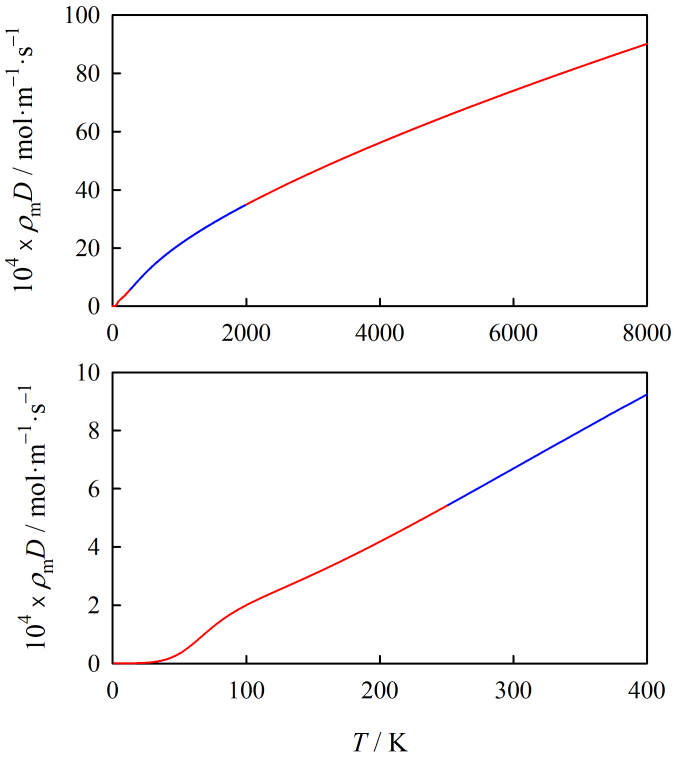

Figure 12: Correlation for the product of molar density and binary diffusion coefficient of an equimolar (H_2O + CO_2) mixture in the dilute gas limit as given by Eqs. (11) and (12). The correlation is colored in blue within its range of validity and in red outside of this range.

figurations of the two molecules. The PES is represented analytically by a site–site potential function with nine sites for H_2O and seven sites for CO_2; a Fortran 90 implementation is provided in the Supporting Information. The calculation of the transport properties involves also the like-species interactions; the respective generalized cross sections were obtained in our previous work on pure H_2O [11, 20] and pure CO_2 [3].

The comparison of the calculated values for the H_2O–CO_2 cross second virial coefficient with the available experimental data and previously calculated values [60, 61] based on the PES of Wheatley and Harvey [18] reveals that the present values are probably the most accurate to date. In the case of the transport properties, the predicted values are almost certainly more accurate than the scarce experimental data. Moreover, they cover a much wider temperature range and the full composition range. Thus, they represent a substantial improvement in our knowledge of the transport properties of this mixture.

Tables of calculated values for all four investigated properties are provided together with their estimated uncertainties. In the case of the viscosity and the thermal conductivity, small empirical adjustments in the form of scaling factors are recommended. We also provide practical correlations for the cross second virial coefficient and the binary diffusion coefficient, where we neglected the very small composition dependence of the latter because it should be irrelevant in any applications. Since the calculated transport property values are smooth functions of temperature and mole fraction, values for these properties at temperatures and mole fractions different from those listed in the tables can be determined reliably using a suitable interpolation scheme.

Finally, we note that while the present results and those of our previous studies on eight further binary systems [10, 12–16] cover only the dilute gas phase, they provide an essential basis for the improvement of approaches to estimate mixture properties also at higher densities by enforcing the correct behavior in the dilute gas limit.

Acknowledgments

The author wishes to thank Dr. Allan Harvey for helpful discussions and Dr. Richard Perkins for providing his dilute gas thermal conductivity data for the (H_2O + CO_2) system prior to publication.

Appendix A. Supplementary data

Supplementary data related to this article can be found at

Nomenclature

Abbreviations

calc	calculated
CBS	complete basis set
CCSD(T)	coupled-cluster with single, double, and perturbative triple excitations
cl	classical
corr	correlation
exp	experimental
HF	Hartree–Fock
min	minimum
MP2	second-order Møller–Plesset perturbation theory
MSMC	Mayer-sampling Monte Carlo
PES	potential energy surface

QFH	quadratic Feynman–Hibbs
rec	recommended
RI	resolution of identity
rot	rotational
trans	translational

Symbols

A_{ij}, α_{ij}, b_{ij}, $C_{6\,ij}$	parameters for the interaction between site i in molecule 1 and site j in molecule 2
b_i	parameter of the correlation for the cross second virial coefficient
B_{12}	cross second virial coefficient
d_i	parameter of the correlation for the product of molar density and binary diffusion coefficient
D	binary diffusion coefficient
E	energy
f_6	damping function
$\hbar$	Planck's constant divided by 2π
I_i	moment of inertia perpendicular to the molecular axis of the linear molecule i
$I_{i\alpha}$	moment of inertia for principal axis α of the non-linear molecule i
k	coverage factor
k_B	Boltzmann's constant
N_A	Avogadro's constant
q_i	charge of site i
R, $\mathbf{R}$	separation and separation vector, respectively, between the centers of mass of molecules 1 and 2
R_{ij}	separation between site i in molecule 1 and site j in molecule 2
S	function in the correlation for the product of molar density and binary diffusion coefficient
T	temperature
T^*, $\overline{T}$	reduced temperatures
U	combined expanded uncertainty
V	total interaction energy
V_{ij}	interaction energy between site i in molecule 1 and site j in molecule 2
w	weighting function
x, y, z	Cartesian components of $\mathbf{R}$
x_i	mole fraction of component i
X	cardinal number of a basis set
$[X]_n$	transport property X with $X \in \{\eta, \lambda, \rho_\mathrm{m} D\}$ in the nth-order kinetic theory approximation
α	parameter in the CBS extrapolation scheme
η	shear viscosity
λ	thermal conductivity
μ	reduced mass of molecules 1 and 2
ρ_m	molar density
ϕ_{12}	dilute gas cross isothermal Joule–Thomson coefficient
$\psi_{i\alpha}$	angle of rotation around principal axis α of molecule i
Ω_i	angular orientation of molecule i

References

[1] K. Patkowski, W. Cencek, P. Jankowski, K. Szalewicz, J. B. Mehl, G. Garberoglio, A. H. Harvey, Potential energy surface for interactions between two hydrogen molecules, J. Chem. Phys. 129 (9) (2008) 094304. doi:10.1063/1.2975220.

[2] R. Hellmann, *Ab initio* potential energy surface for the nitrogen molecule pair and thermophysical properties of nitrogen gas, Mol. Phys. 111 (3) (2013) 387–401. doi:10.1080/00268976.2012.726379.

[3] R. Hellmann, *Ab initio* potential energy surface for the carbon dioxide molecule pair and thermophysical properties of dilute carbon dioxide gas, Chem. Phys. Lett. 613 (2014) 133–138. doi:10.1016/j.cplett.2014.08.057.

[4] R. Bukowski, K. Szalewicz, G. C. Groenenboom, A. van der Avoird, Predictions of the Properties of Water from First Principles, Science 315 (5816) (2007) 1249–1252. doi:10.1126/science.1136371.

[5] R. Bukowski, K. Szalewicz, G. C. Groenenboom, A. van der Avoird, Polarizable interaction potential for water from coupled cluster calculations. I. Analysis of dimer potential energy surface, J. Chem. Phys. 128 (9) (2008) 094313. doi:10.1063/1.2832746.

[6] R. Hellmann, E. Bich, E. Vogel, V. Vesovic, *Ab initio* intermolecular potential energy surface and thermophysical properties of hydrogen sulfide, Phys. Chem. Chem. Phys. 13 (30) (2011) 13749–13758. doi:10.1039/C1CP20873J.

[7] F. R. W. McCourt, J. J. M. Beenakker, W. E. Köhler, I. Kuščer, Nonequilibrium Phenomena in Polyatomic Gases, Vol. I: Dilute Gases, Clarendon Press, Oxford, 1990.

[8] A. S. Dickinson, R. Hellmann, E. Bich, E. Vogel, Transport properties of asymmetric-top molecules, Phys. Chem. Chem. Phys. 9 (22) (2007) 2836–2843. doi:10.1039/B618549E.

[9] E. Bich, J. B. Mehl, R. Hellmann, V. Vesovic, Dilute Gases, in: M. J. Assael, A. R. H. Goodwin, V. Vesovic, W. A. Wakeham (Eds.), Experimental Thermodynamics Volume IX: Advances in Transport Properties of Fluids, The Royal Society of Chemistry, Cambridge, 2014, Ch. 7, pp. 226–252. doi:10.1039/9781782625254-00226.

[10] R. Hellmann, E. Bich, E. Vogel, V. Vesovic, Intermolecular potential energy surface and thermophysical properties of the CH_4–N_2 system, J. Chem. Phys. 141 (22) (2014) 224301. doi:10.1063/1.4902807.

[11] R. Hellmann, E. Bich, An improved kinetic theory approach for calculating the thermal conductivity of polyatomic gases, Mol. Phys. 113 (2) (2015) 176–183. doi:10.1080/00268976.2014.951703.

[12] R. Hellmann, E. Bich, V. Vesovic, Calculation of the thermal conductivity of low-density CH_4–N_2 gas mixtures using an improved kinetic theory approach, J. Chem. Phys. 144 (13) (2016) 134301. doi:10.1063/1.4945014.

[13] R. Hellmann, E. Bich, V. Vesovic, Cross second virial coefficients and dilute gas transport properties of the (CH_4 + CO_2), (CH_4 + H_2S), and (H_2S + CO_2) systems from accurate intermolecular potential energy surfaces, J. Chem. Thermodyn. 102 (2016) 429–441. doi:10.1016/j.jct.2016.07.034.

[14] R. Hellmann, Cross Second Virial Coefficients and Dilute Gas Transport Properties of the (CH_4 + C_3H_8) and (CO_2 + C_3H_8) Systems from Accurate Intermolecular Potential Energy Surfaces, J. Chem. Eng. Data 63 (1) (2018) 246–257. doi:10.1021/acs.jced.7b00886.

[15] J.-P. Crusius, R. Hellmann, J. C. Castro-Palacio, V. Vesovic, *Ab initio* intermolecular potential energy surface for the CO_2—N_2 system and related thermophysical properties, J. Chem. Phys. 148 (21) (2018) 214306. doi:10.1063/1.5034347.

[16] R. Hellmann, Thermophysical Properties of Gaseous H_2S–N_2 Mixtures from First-Principles Calculations, Z. Phys. Chem., published online. doi:10.1515/zpch-2018-1250.

[17] J. Makarewicz, Intermolecular potential energy surface of the water-carbon dioxide complex, J. Chem. Phys. 132 (23) (2010) 234305. doi:10.1063/1.3439693.

[18] R. J. Wheatley, A. H. Harvey, Intermolecular potential energy surface and second virial coefficients for the water–CO_2 dimer, J. Chem. Phys. 134 (13) (2011) 134309. doi:10.1063/1.3574345.

[19] Q. K. Wang, J. M. Bowman, Two-component, *ab initio* potential energy surface for CO_2—H_2O, extension to the hydrate clathrate, CO_2@$(H_2O)_{20}$, and VSCF/VCI vibrational analyses of both, J. Chem. Phys. 147 (16) (2017) 161714. doi:10.1063/1.4994543.

[20] R. Hellmann, E. Vogel, The Viscosity of Dilute Water Vapor Revisited: New Reference Values from Experiment and Theory for Temperatures between (250 and 2500) K, J. Chem. Eng. Data 60 (12) (2015) 3600–3605. doi:10.1021/acs.jced.5b00599.

[21] E. M. Mas, K. Szalewicz, Effects of monomer geometry and basis set saturation on computed depth of water dimer potential, J. Chem. Phys.

104 (19) (1996) 7606–7614. doi:10.1063/1.471469.

[22] S. F. Boys, F. Bernardi, The calculation of small molecular interactions by the differences of separate total energies. Some procedures with reduced errors, Mol. Phys. 19 (4) (1970) 553–566. doi:10.1080/00268977000101561.

[23] F. Weigend, M. Häser, RI-MP2: first derivatives and global consistency, Theor. Chem. Acc. 97 (1-4) (1997) 331–340. doi:10.1007/s002140050269.

[24] F. Weigend, M. Häser, H. Patzelt, R. Ahlrichs, RI-MP2: optimized auxiliary basis sets and demonstration of efficiency, Chem. Phys. Lett. 294 (1-3) (1998) 143–152. doi:10.1016/S0009-2614(98)00862-8.

[25] F. Weigend, M. Kattannek, R. Ahlrichs, Approximated electron repulsion integrals: Cholesky decomposition versus resolution of the identity methods, J. Chem. Phys. 130 (16) (2009) 164106. doi:10.1063/1.3116103.

[26] S. Kossmann, F. Neese, Comparison of two efficient approximate Hartee–Fock approaches, Chem. Phys. Lett. 481 (4-6) (2009) 240–243. doi:10.1016/j.cplett.2009.09.073.

[27] T. H. Dunning, Jr., Gaussian basis sets for use in correlated molecular calculations. I. The atoms boron through neon and hydrogen, J. Chem. Phys. 90 (2) (1989) 1007–1023. doi:10.1063/1.456153.

[28] R. A. Kendall, T. H. Dunning, Jr., R. J. Harrison, Electron affinities of the first-row atoms revisited. Systematic basis sets and wave functions, J. Chem. Phys. 96 (9) (1992) 6796–6806. doi:10.1063/1.462569.

[29] F. Weigend, A fully direct RI-HF algorithm: Implementation, optimised auxiliary basis sets, demonstration of accuracy and efficiency, Phys. Chem. Chem. Phys. 4 (18) (2002) 4285–4291. doi:10.1039/B204199P.

[30] F. Weigend, A. Köhn, C. Hättig, Efficient use of the correlation consistent basis sets in resolution of the identity MP2 calculations, J. Chem. Phys. 116 (8) (2002) 3175–3183. doi:10.1063/1.1445115.

[31] K. Patkowski, On the accuracy of explicitly correlated coupled-cluster interaction energies — have orbital results been beaten yet?, J. Chem. Phys. 137 (3) (2012) 034103. doi:10.1063/1.4734597.

[32] A. Halkier, T. Helgaker, P. Jørgensen, W. Klopper, H. Koch, J. Olsen, A. K. Wilson, Basis-set convergence in correlated calculations on Ne, N_2, and H_2O, Chem. Phys. Lett. 286 (3-4) (1998) 243–252. doi:10.1016/S0009-2614(98)00111-0.

[33] K. Raghavachari, G. W. Trucks, J. A. Pople, M. Head-Gordon, A fifth-order perturbation comparison of electron correlation theories, Chem. Phys. Lett. 157 (6) (1989) 479–483. doi:10.1016/S0009-2614(89)87395-6.

[34] F. Neese, The ORCA program system, WIREs Comput. Mol. Sci. 2 (1) (2012) 73–78. doi:10.1002/wcms.81.

[35] CFOUR, Coupled-Cluster techniques for Computational Chemistry, a quantum-chemical program package by J. F. Stanton, J. Gauss, M. E. Harding, P. G. Szalay with contributions from A. A. Auer, R. J. Bartlett, U. Benedikt, C. Berger, D. E. Bernholdt, Y. J. Bomble, L. Cheng, O. Christiansen, M. Heckert, O. Heun, C. Huber, T.-C. Jagau, D. Jonsson, J. Jusélius, K. Klein, W. J. Lauderdale, D. A. Matthews, T. Metzroth, L. A. Mück, D. P. O'Neill, D. R. Price, E. Prochnow, C. Puzzarini, K. Ruud, F. Schiffmann, W. Schwalbach, S. Stopkowicz, A. Tajti, J. Vázquez, F. Wang, J. D. Watts and the integral packages MOLECULE (J. Almlöf and P. R. Taylor), PROPS (P. R. Taylor), ABACUS (T. Helgaker, H. J. Aa. Jensen, P. Jørgensen, and J. Olsen), and ECP routines by A. V. Mitin and C. van Wüllen. For the current version, see http://www.cfour.de.

[36] K. T. Tang, J. P. Toennies, An improved simple model for the van der Waals potential based on universal damping functions for the dispersion coefficients, J. Chem. Phys. 80 (8) (1984) 3726–3741. doi:10.1063/1.447150.

[37] A. K. Wilson, T. van Mourik, T. H. Dunning, Jr., Gaussian basis sets for use in correlated molecular calculations. VI. Sextuple zeta correlation consistent basis sets for boron through neon, J. Mol. Struct.: THEOCHEM 388 (1996) 339–349. doi:10.1016/S0166-1280(96)80048-0.

[38] R. P. Feynman, A. R. Hibbs, Quantum Mechanics and Path Integrals, McGraw-Hill, New York, 1965.

[39] J. K. Singh, D. A. Kofke, Mayer Sampling: Calculation of Cluster Integrals using Free-Energy Perturbation Methods, Phys. Rev. Lett. 92 (22) (2004) 220601. doi:10.1103/PhysRevLett.92.220601.

[40] B. Jäger, R. Hellmann, E. Bich, E. Vogel, *Ab initio* virial equation of state for argon using a new nonadditive three-body potential, J. Chem. Phys. 135 (8) (2011) 084308. doi:10.1063/1.3627151.

[41] L. Waldmann, Transporterscheinungen in Gasen von mittlerem Druck, in: S. Flügge (Ed.), Handbuch der Physik, Vol. 12, Springer-Verlag, Berlin, 1958, pp. 295–514. doi:10.1007/978-3-642-45892-7_4.

[42] L. Waldmann, E. Trübenbacher, Formale kinetische Theorie von Gasgemischen aus anregbaren Molekülen, Z. Naturforsch. A 17 (5) (1962) 363–376. doi:10.1515/zna-1962-0501.

[43] J. H. Ferziger, H. G. Kaper, The Mathematical Theory of Transport Processes in Gases, North-Holland, Amsterdam, 1972.

[44] C. F. Curtiss, Classical, diatomic molecule, kinetic theory cross sections, J. Chem. Phys. 75 (3) (1981) 1341–1346. doi:10.1063/1.442140.

[45] M. Mustafa, Measurement and Calculation of Transport Properties of Polyatomic Gases, Ph.D. thesis, Imperial College London, London, UK (1987).

[46] E. L. Heck, A. S. Dickinson, Transport and relaxation cross-sections for pure gases of linear molecules, Comput. Phys. Commun. 95 (2-3) (1996) 190–220. doi:10.1016/0010-4655(96)00033-1.

[47] R. Span, W. Wagner, A New Equation of State for Carbon Dioxide Covering the Fluid Region from the Triple Point Temperature to 1100 K at Pressures up to 800 MPa, J. Phys. Chem. Ref. Data 25 (6) (1996) 1509–1596. doi:10.1063/1.555991.

[48] W. Wagner, A. Pruß, The IAPWS Formulation 1995 for the Thermodynamic Properties of Ordinary Water Substance for General and Scientific Use, J. Phys. Chem. Ref. Data 31 (2) (2002) 387–535. doi:10.1063/1.1461829.

[49] R. Hellmann, Reference Values for the Second Virial Coefficient and Three Dilute Gas Transport Properties of Ethane from a State-of-the-Art Intermolecular Potential Energy Surface, J. Chem. Eng. Data 63 (2) (2018) 470–481. doi:10.1021/acs.jced.7b01069.

[50] E. L. Heck, A. S. Dickinson, Transport and relaxation properties of N_2, Mol. Phys. 81 (6) (1994) 1325–1352. doi:10.1080/00268979400100911.

[51] A. D. King, Jr., C. R. Coan, Solubility of water in compressed carbon dioxide, nitrous oxide, and ethane. Evidence for hydration of carbon dioxide and nitrous oxide in the gas phase, J. Am. Chem. Soc. 93 (8) (1971) 1857–1862. doi:10.1021/ja00737a004.

[52] C. J. Wormald, C. N. Colling, Excess enthalpies of some mixtures containing steam, in: Proc. 9th Int. Conf. Prop. Steam, Pergamon, Oxford, 1980, pp. 655–663.

[53] C. E. Vanderzee, N. C. Haas, Second cross virial coefficients B_{12} for gas mixture (carbon dioxide+water) from 300 to 1000 K, J. Chem. Thermodyn. 13 (3) (1981) 203–211. doi:10.1016/0021-9614(81)90119-1.

[54] C. J. Wormald, C. N. Colling, G. Smith, Thermodynamics of supercritical steam + carbon dioxide mixtures, Fluid Phase Equilib. 10 (2-3) (1983) 223–231. doi:10.1016/0378-3812(83)80036-3.

[55] G. R. Smith, C. J. Wormald, The excess molar enthalpies of $\{xH_2O + (1-x)CO\}$(g) and $\{xH_2O + (1-x)CO_2\}$(g), J. Chem. Thermodyn. 16 (6) (1984) 543–550. doi:10.1016/0021-9614(84)90005-3.

[56] M. R. Patel, J. C. Holste, K. R. Hall, P. T. Eubank, Thermophysical properties of gaseous carbon dioxide–water mixtures, Fluid Phase Equilib. 36 (1987) 279–299. doi:10.1016/0378-3812(87)85029-X.

[57] C. J. Wormald, N. M. Lancaster, Excess enthalpies and cross-term second virial coefficients for mixtures containing water vapour, J. Chem. Soc., Faraday Trans. 1 84 (9) (1988) 3141–3158. doi:10.1039/F19888403141.

[58] A. Bamberger, G. Sieder, G. Maurer, High-pressure (vapor+liquid) equilibrium in binary mixtures of (carbon dioxide+water or acetic acid) at temperatures from 313 to 353 K, J. Supercrit. Fluids 17 (2) (2000) 97–110. doi:10.1016/S0896-8446(99)00054-6.

[59] C. W. Meyer, A. H. Harvey, Dew-Point Measurements for Water in Compressed Carbon Dioxide, AIChE J. 61 (9) (2015) 2913–2925. doi:10.1002/aic.14818.

[60] A. J. Schultz, D. A. Kofke, A. H. Harvey, Molecular-Based Virial Coefficients of CO_2-H_2O Mixtures, AIChE J. 61 (9) (2015) 3029–3037. doi:10.1002/aic.14880.

[61] R. J. Wheatley, A. H. Harvey, Erratum: "Intermolecular potential energy surface and second virial coefficients for the water–CO_2 dimer" [J. Chem. Phys. 134, 134309 (2011)], J. Chem. Phys. 145 (18) (2016) 189901. doi:10.1063/1.4967488.

[62] N. M. Lancaster, C. J. Wormald, Excess Molar Enthalpies of Nine Binary Steam Mixtures: New and Corrected Values, J. Chem. Eng. Data 35 (1)

(1990) 11–16. doi:10.1021/je00059a004.

[63] G. Garberoglio, P. Jankowski, K. Szalewicz, A. H. Harvey, Fully quantum calculation of the second and third virial coefficients of water and its isotopologues from ab initio potentials, Faraday Discuss. Advance Article. doi:10.1039/C8FD00092A.

[64] S. Bock, E. Bich, E. Vogel, A. S. Dickinson, V. Vesovic, Calculation of the transport properties of carbon dioxide. II. Thermal conductivity and thermomagnetic effects, J. Chem. Phys. 120 (17) (2004) 7987–7997. doi:10.1063/1.1687312.

[65] B. Jäger, E. Bich, Thermophysical properties of krypton-helium gas mixtures from *ab initio* pair potentials, J. Chem. Phys. 146 (21) (2017) 214302. doi:10.1063/1.4984100.

[66] F. Munczak, M. Sedlacek, The influence of water vapour on the viscosity of He, Ar, N_2 and CO_2 at 30°C, Physica 46 (1) (1970) 1–7. doi:10.1016/0031-8914(70)90111-4.

[67] D. L. Timrot, N. B. Vargaftik, Heat conductivity, viscosity, and thermodynamical properties of steam at high tempertures and pressures, in: Transactions of the 4th World Power Conference, Vol. III, Lund Humphries, London, 1952, pp. 1642–1666.

[68] K. M. Dijkema, J. C. Stouthart, D. A. de Vries, Measurements of the thermal conductivity of gases and gas mixtures, methods and results, Wärme- und Stoffübertrag. 5 (1) (1972) 47–55. doi:10.1007/BF01000478.

[69] R. A. Perkins, paper in preparation (private communication, November 2018).

[70] J. W. Haarman, Thermal Conductivity Measurements of He, Ne, Ar, Kr, N_2 and CO_2 with a Transient Hot Wire Method, Am. Inst. Phys. Conf. Proc. 11 (1) (1973) 193–202. doi:10.1063/1.2948425.

[71] A. Winkelmann, Ueber die Diffusion von Gasen und Dämpfen, Ann. Phys. 258 (6) (1884) 152–161. doi:10.1002/andp.18842580603.

[72] A. Winkelmann, Ueber den Einfluss der Temperatur auf die Verdampfung und auf die Diffusion von Dämpfen, Ann. Phys. 272 (1) (1889) 93–114. doi:10.1002/andp.18882720105.

[73] M. Trautz, W. Müller, Die Reibung, Wärmeleitung und Diffusion in Gasmischungen XXXIII. Die Korrektion der bisher mit der Verdampfungsmethode gemessenen Diffusionskonstanten, Ann. Phys. 414 (4) (1935) 333–352. doi:10.1002/andp.19354140404.

[74] F. A. Schwertz, J. E. Brow, Diffusivity of Water Vapor in Some Common Gases, J. Chem. Phys. 19 (5) (1951) 640–646. doi:10.1063/1.1748306.

[75] K. Rossié, Die Diffusion von Wasserdampf in Luft bei Temperaturen bis 300°C, Forsch. Ing.-Wes. 19 (2) (1953) 49–58. doi:10.1007/BF02558326.

[76] W. L. Crider, The Use of Diffusion Coefficients in the Measurement of Vapor Pressure, J. Am. Chem. Soc. 78 (5) (1956) 924–925. doi:10.1021/ja01586a015.

[77] I. Nagata, T. Hasegawa, Gaseous interdiffusion coefficients, J. Chem. Eng. Jpn. 3 (2) (1970) 143–145. doi:10.1252/jcej.3.143.

[78] M. Schmidt, H. Lipson, Distilling Free-Form Natural Laws from Experimental Data, Science 324 (5923) (2009) 81–85. doi:10.1126/science.1165893.